Supporting Information

Engineered paramagnetic graphene quantum dots with enhanced relaxivity for tumor imaging

Yuqi Yang,[†,‡] Shizhen Chen, [†,‡] Haidong Li, [‡] Yaping Yuan,[‡] Zhiying Zhang, [‡] Junshuai Xie,[‡] Dennis W. Hwang,[§] Aidong Zhang [‖] , Maili Liu[‡] and Xin Zhou*[,‡]

([+] Co-first authors contributed equally to this work)

‡Key Laboratory of Magnetic Resonance in Biological Systems, State Key Laboratory of Magnetic Resonance and Atomic and Molecular Physics, National Center for Magnetic Resonance in Wuhan, Wuhan Institute of Physics and Mathematics, Chinese Academy of Sciences, Wuhan, 430071, P. R. China.

§ Department of Chemistry & Biochemistry, National Chung-Cheng University, 168 University Rd., Min-Hsiung, Chiayi 621, Taiwan

‖ Aidong Zhang
Key Laboratory of Pesticide and Chemical Biology of Ministry of Education,
College of Chemistry, Central China Normal University, Wuhan 430079, PR China

Corresponding Author * E-mail: xinzhou@wipm.ac.cn , Tel:+86-027-87198802
Author Contributions † Y. Y. and S. C. contributed equally to this work.

1. Synthetic protocols 3
1.1. Synthesis of graphene quantum dots (GQD) 3
1.2. Synthesis of PGQD-HA 3
Figure S1. The synthetic procedure of DOX/PGQD-HA 4
2. Characterization 4
Figure S2. High-resolution XPS C1s spectra of GQD 4
Figure S3. XPS spectra of GQD (red) and PGQD-HA (black) 5
Figure S4. FTIR spectra of the PGQD-HA, PGQD and GQD. 5
Figure S5. Photoluminescence spectra 6
Figure S6. The longitudinal relaxivity (r_1) of PGQD-HA 7
3. Cellular uptake of PGQD-HA 7
Figure S7. TEM of lung cancer cells 7
4. Cellular MRI 7
Figure S8. T_1-weighted magnetic resonance images 8
Figure S9. T_1-weighted magnetic resonance images of A549 cells 8
5. In Vivo MRI 8
Figure S10. *In vivo* T_1-weighted magnetic resonance image 9
6. DOX loading and releasing 9
Figure S11. Photoluminescence spectra. 10
Figure S12. Electrode reaction of doxorubicin 10
Figure S13. Cyclic voltammetry curves. 11
Figure S14. DOX release. 11
7. Isotherms characterizing adsorption of DOX onto GQD 11
Figure S15. Adsorption isotherms of DOX on GQD at different temperatures. 12
8. Cell viability assay 12
Figure S16. Cell viability. 13

1. Synthetic protocols

1.1. Synthesis of graphene quantum dots (GQD)

Graphene oxide (GO, 40 mg) was suspended in a mixture of 98% sulfuric acid (30 mL) and fuming nitric acid (10 mL) by sonication. The solution was stirred at 80 °C for 5 h and then refluxed at 110 °C for 20 h. The mixture was cooled to room temperature and diluted with 400mL of deionized water. The obtained solution was antagonized by K_2CO_3 and then centrifuged at 20000 rpm for 30 min. The resulting supernatant was further dialyzed in a dialysis bag (retained molecular weight: 3500 Da) until all the resulting salt was removed.

1.2. Synthesis of PGQD-HA

1 mM (191 mg) EDC and 10mg GQD were placed in a 50 mL round-bottom flask with 10 mL distilled water. The pH was adjusted to 5.0 by 0.1 mM HCl. After 10 min sonication and 2 h stirring at room temperature, pH was then adjusted to 8.0 by 0.1 mM NaOH. Then 0.25 mM (29 mg) NHS and 0.02 mM Boc-NH-PEG-NH_2 in 10 mL DMF was added. The mixture was stirred for another 24 h at room temperature. The produced GQD-PEG-NH-Boc solution was purified by dialysis against distilled water. The resulted solution was evaporated and re-dispersed in 10 mL TFA and stirred for 2h at room temperature. The solvent was removed by evaporation and the resulted GQD-PEG-NH_2 was purified by dialysis against distilled water. DOTA was further modified to the GQD-PEG-NH_2 nanoparticles by reaction between the carboxyl groups of DOTA and the amino groups of PEG. Thereafter, $GdCl_3 \cdot 6H_2O$ (7.4 mg, 0.02 mM) was added to an aqueous solution of GQD-PEG-DOTA for chelating. The mixture was maintained at pH 5.5 and allowed to react for 24 h. The free Gd(III) was removed by dialysis against Milli-Q water using a 3.5 kDa molecular weight cutoff dialysis membrane for 2 days. Finally, the synthesized GQD-PEG-Gd nanoparticles were freeze dried. The Gd(III) content in the product was determined by inductively coupled plasma-mass spectrometry.

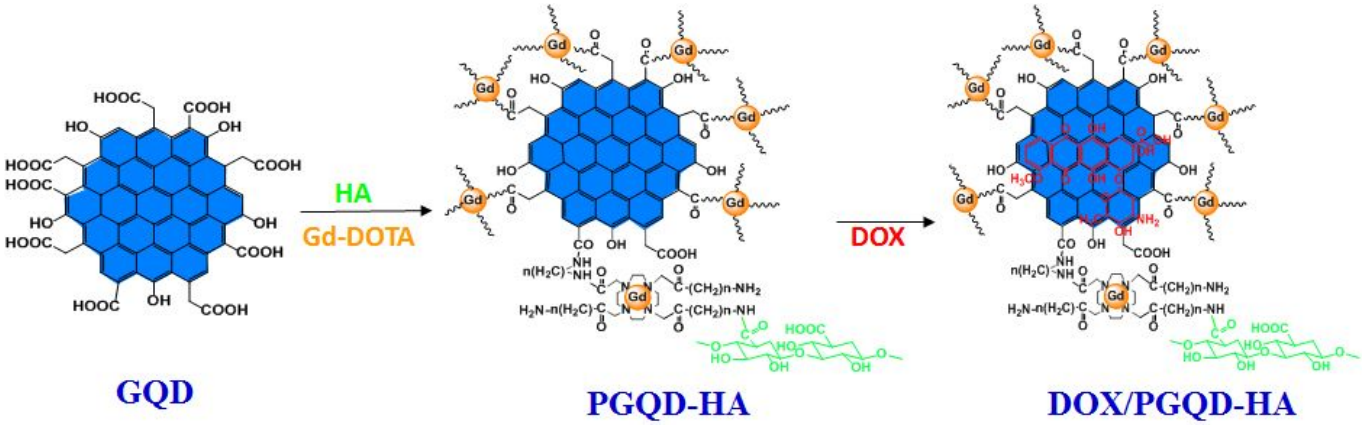

Figure S1. The synthetic procedure of DOX/PGQD-HA

2. Characterization

The presence of C=C, C−O, C=O, and COOH bonds in the high-resolution spectra of C1s **(Figure S2)** indicated that GQD were functionalized with hydroxyl, carbonyl, and carboxylic acid groups.

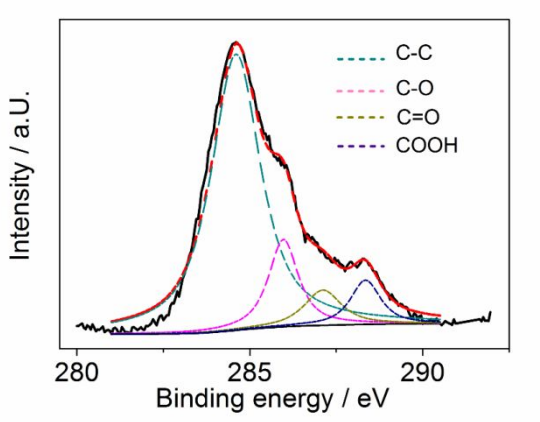

Figure S2. High-resolution XPS C1s spectra of GQD

X-ray photoelectron spectroscopy (XPS) spectra of PGQD-illustrated a new N 1s signal (400 eV) and typical Gd 3d 5/2 (1188 eV) peak (**Figure S3**), indicating the successful modification of Gd-DOTA on PGQD. Inductively coupled plasma mass spectrometry (ICP-MS) analysis suggested that the content of Gd in PGQD-HA is 0.98%.

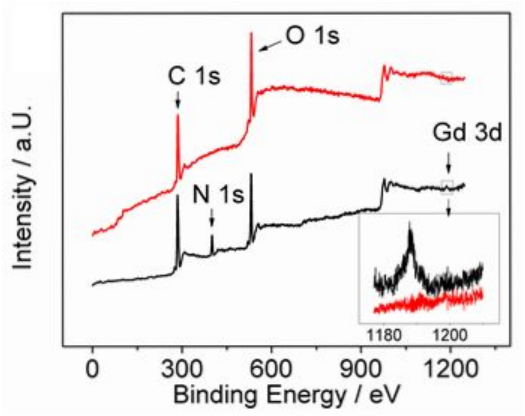

Figure S3. XPS spectra of GQD (red) and PGQD-HA (black)

Figure S4 shows the Fourier transform infrared (FTIR) results of GQD, PGQD and PGQD-HA. The FTIR spectrum of GQD demonstrates the presence of C–O (C–O at 1100 cm^{-1}), C–OH (C–OH at 1382 cm^{-1}), C=O in carboxylic acid and carbonyl moieties (C=O at 1639 cm^{-1}) and the H-bonded associated OH (broad band around 3437 cm^{-1}). After Gd-DOTA was linked to GQD via a bridge of diamino-terminated poly (ethylene glycol) (PEG diamine), the band at 1382, 1639 and 1726 cm^{-1} almost disappears while the band at 3437 cm^{-1} decays significantly in the FTIR spectrum of PGQD, indicating the amidation of carboxylic acid. New peaks at 1037 and 2951 cm^{-1} are assigned to the C–N in-plane and N-H in-plane stretching of amine groups, indicating the successful introduction of nitrogen in the PGQD. The FTIR spectrum of the PGQD-HA shows stonger H-bonded associated OH (broad band around 3437 cm^{-1}) than PGQD, and the band at 1037 (C–N) and 2951 cm^{-1} (N-H) almost disappears, demonstrating the succesful introducing of HA.

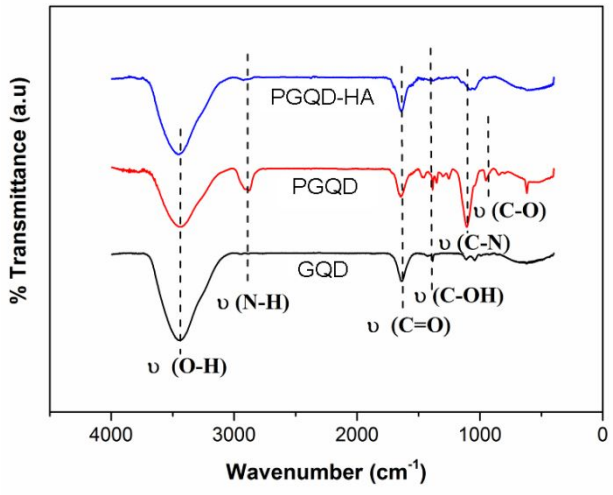

Figure S4. FTIR spectra of the PGQD-HA, PGQD and GQD.

Similar as other fluorescent carbon-based nanomaterials,[18] the emission spectra of the prepared GQD also showed an excitation-dependent feature. The emission peak shift from 465 nm to 510 nm accompanied by the remarkably decrease in emission intensity as the excitation wavelength varies from 360 nm to 430 nm (**Figure S5a**). This phenomenon may result from optical selection of differently sized GQD and surface defects of GQD. The obtained GQD were further modified with Gd-DOTA and HA through a linkage of PEG-diamine. **Figure S5b** illustrates the PL emission spectra of GQD and PGQD-HA aqueous solution with excitation from a 360 nm laser. The maximum PL position red shifted 30 nm after further modifications and the PL intensity decreased.

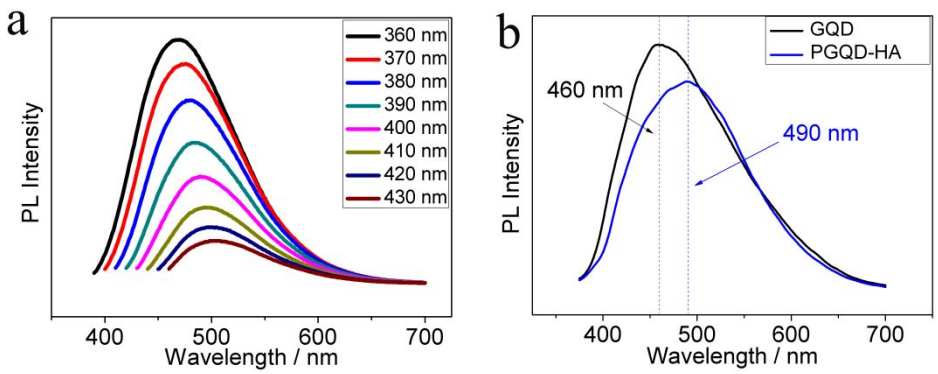

Figure S5. (a) Photoluminescence spectra of GQD aqueous solution under different excitation wavelength. (b) Photoluminescence spectra of GQD and PGQD-HA aqueous solution under an exciting wavelength of 360 nm.

The longitudinal relaxivities of the PGQD-HA and the commercial available MR contrast agent Gd-DOTA were determined on a Bruker Biospec MRI scanner in according to the equation of $r_1 = (1/T_1 \text{ sample} - 1/T_1 \text{ PBS})/[Gd]$. The T_1 values of selected compounds with four different concentrations in PBS were measured with a 9.4 T MR spectrometer at 25 °C. The ($1/T_1$ sample-$1/T_1$ PBS) values of nanoprobes with corresponding Gd^{3+} concentrations measured by ICP-MS provided the relaxivity were plotted. The r_1 value of the PGQD-HA was 68.9 $mM^{-1}s^{-1}$, which was 16 times higher than that of the Gd-DOTA when calculated on the basis of the concentration of Gd ions.

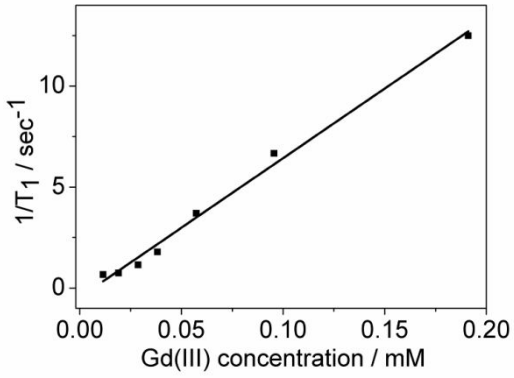

Figure S6. The longitudinal relaxivity (r_1) of PGQD-HA. Linear plots of 0.002，0.004，0.006, 0.01, 0.02, 0.04 mM Gd versus ($1/T_1$ sample-$1/T_1$ PBS)

3. Cellular uptake of PGQD-HA

PGQD-HA were transported into A549 cells by receptor-mediated endocytosis through the high affinity between the modified HA in PGQD-HA and the overexpressed CD44 receptor in the plasma membrane of A549 cells. After 3 h incubation, PGQD-HA nanoparticles (black dots in white bubbles) were endocytosed in A549 cells and stored in endosomes (**Figure S7b**). Then, PGQD-HA containing endosomes could fuse with acidic lysosomes and digested by hydrilytic enzymes (**Figure S7c**).

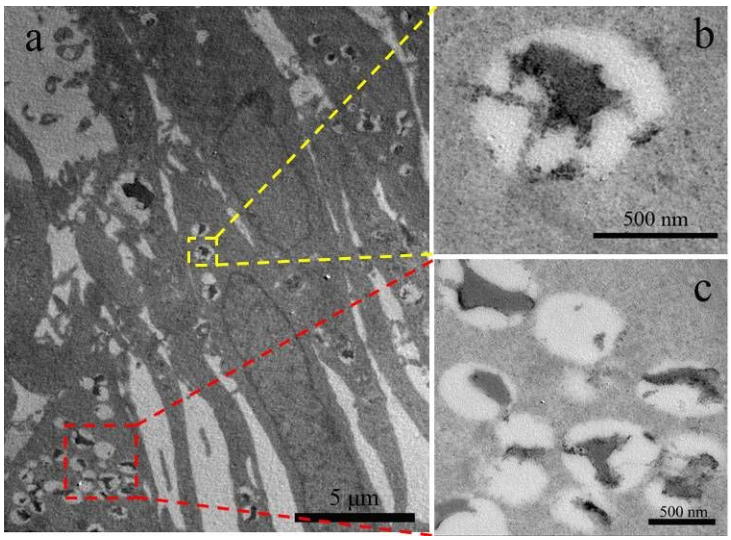

Figure S7. (a) TEM of lung cancer cells (A549) after 3h incubation with 50 μg/mL PGQD-HA. (b) PGQD-HA nanoparticles (black dots) in endosome. (c) PGQD-HA containing endosomes fuse with lysosomes (white bubbles without black dots.)

4. Cellular MRI

A549 cells and MRC-5 cells were cultured in incubation medium for 24 h, in 50 mL of culture flask. PGQD-HA was added to the incubation medium to obtain the certain concentration. All MRI experiments were performed on a 9.4 T microimaging system (Bruker Biospec, Germany) with a 10 mm inner diameter coil for both radiofrequency transmission and reception. NMR spectroscopy was used to determine the T1 relaxation with an inversion recovery pulse sequence, in order to optimize the parameters for the best contrast MR images.

Aqueous solutions of DOX/GQD-Gd-HA were prepared as described in the relaxivity measurement section. The cell lysates were imaged by the same procedure as solutions. Parameters for the images were FOV (field of view)＝20×20 mm^2,TR=200 ms, TE=10 ms for T_1 weighted (T_1W) images. For all images a spin echo sequence was used with a field view (FOV) of 2 cm^2, and a 256 × 256 matrix. All raw data were processed using the Matlab (Mathworks, Natick, MA).

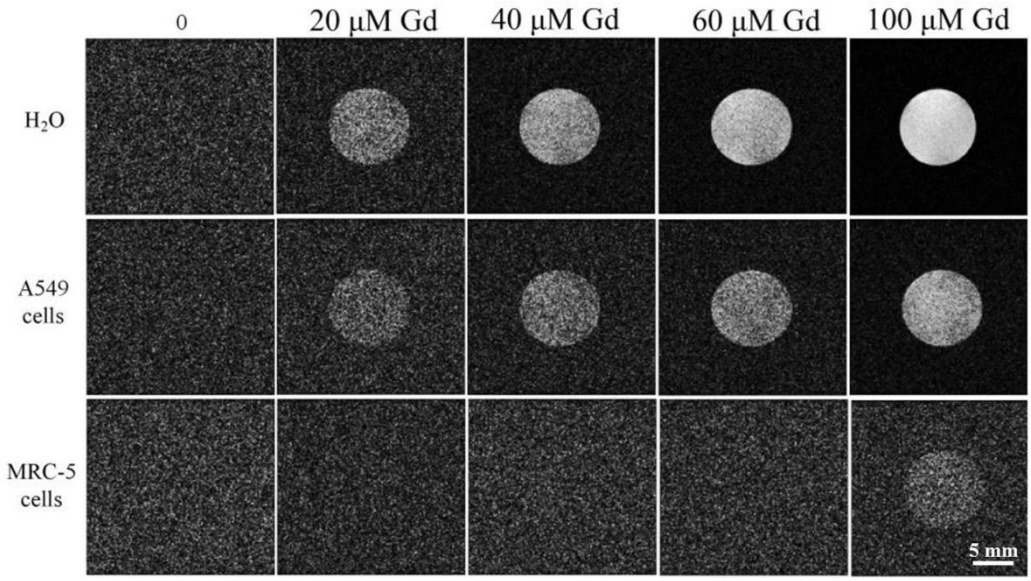

Figure S8. T_1-weighted magnetic resonance images (TR = 80 ms, TE = 10 ms, FOV=2×2 cm^2, Matrix size=128×128) of PGQD-HA water, A549 cells and MRC-5 cells with different Gd concentrations.

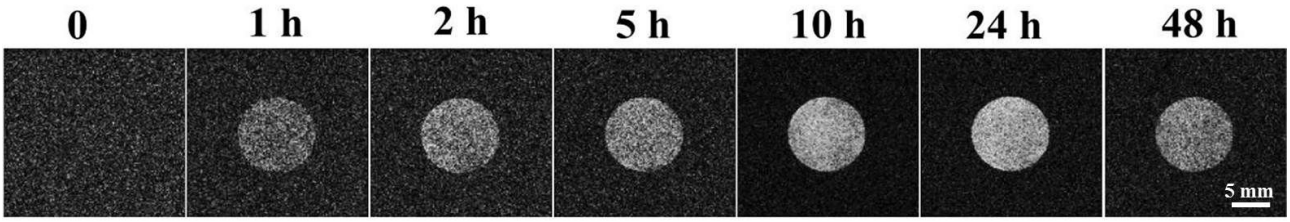

Figure S9. T_1-weighted magnetic resonance images of A549 cells incubated with the DOX/PGQD-HA nanoparticle for different time. (TR=200 ms, TE=10 ms, SI=20 mm, FOV=2×2 cm^2, Matrix size=128×128)

5. *In Vivo* MRI

Imaging was performed using a 7 T small animal horizontal bore system (Bruker BioSpec; Bruker, Billerica, MA). 12-cm-diameter Helmholtz coil arrangement served for rf excitation, whereas signal detection was achieved with a 23-mm diameter surface coil. The coils were decoupled from each other. Gradients used in the magnet were 12 cm diameter at 25 G/cm. Imaging was performed using a custom-built 50 mm diameter send-receive birdcage volume coil. Following

induction of a mouse to the plane of anesthesia using 4% isoflurane/oxygen, mice were fixed to an acrylic patient bed in the prone position and maintained on a 1% isoflurane/oxygen mixture. Body temperature was monitored with a platinum rectal probe connected to a small-animal monitoring system (SA Incorporated) and maintained using a stream of heated air. T_1-weighted images were acquired in the axial plane using a multi-slice spin-echo sequence with the following parameters: TR/TE = 500/15 milliseconds, matrix =128 ×128, FOV (field of view) = 30 ×30 mm, slice thickness = 1 mm, NEX (number of excitations) = 4. Scans were completed 1, 4 and 24 hours after injection of DNCs or dendrimers, as described above.

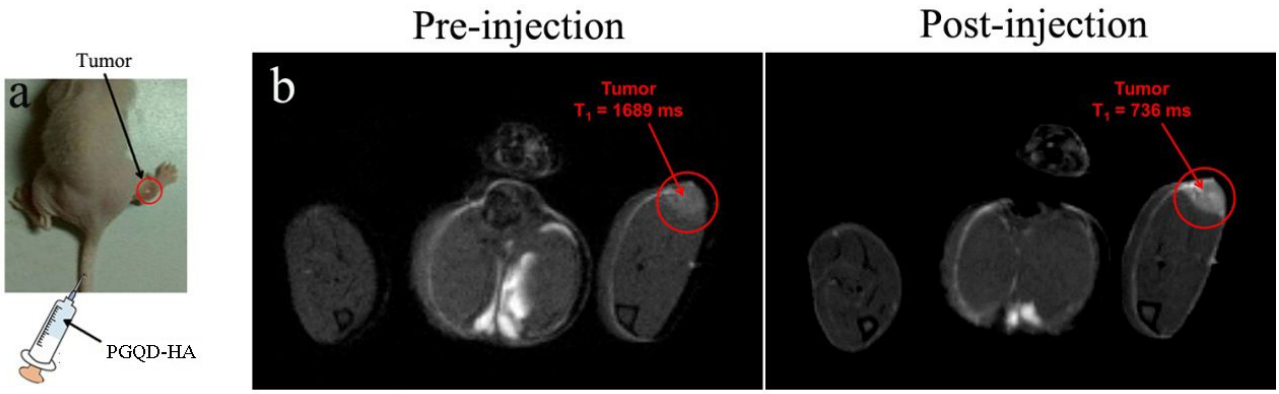

Figure S10. (a) Intravenous tail-vein injection of the PGQD-HA into a mouse with a non-small cell lung tumor in its right leg region. (b) *In vivo* T_1-weighted magnetic resonance image of A549 tumor-bearing mice prior to and 2h post-injection of intravenous injection of PGQD-HA in small animal MRI scanner. The PGQD-HA treated mice showed shortened T_1 relaxation times and strong signal in tumors 2 h post-injection, indicating that there was a significant uptake of nanoprobes. (TR = 400 ms, TE = 10 ms)

6. DOX loading and releasing

4 mL 0.5 mg/mL PGQD-HA in distilled water was mixed with DOX in DMF. The suspension was sonicated for 1 h and then stirred overnight in the dark at room temperature overnight. The obtained solution was dialyzed against PBS 7.4 buffer solution to remove the unbounded DOX and free DMF. Finally, the formed DOX/PGQD-HA complex solution was preserved in darkness at 4 °C.

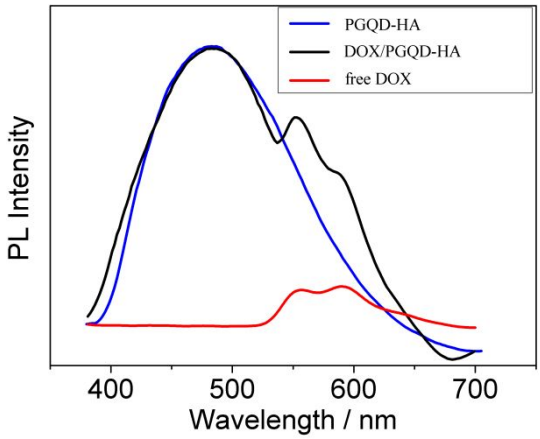

Figure S11. Photoluminescence spectra of free DOX (red), PGQD-HA (blue) and DOX/PGQD-HA (black) with an exciting wavelength of 360 nm.

In addition to the maximum fluorescent emission of GQD-Gd-HA at 490 nm, two new and smaller peaks from DOX at 552 nm and 589 nm arise when DOX/PGQD-HA aqueous solution is irradiated with a 360 nm laser (**Figure S11**).

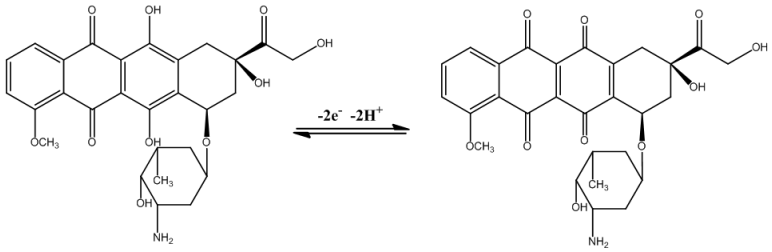

Figure S12. Electrode reaction of doxorubicin

Since its hydroquinone group can be electrochemically oxidized and deoxidized, DOX can also be detected by electrochemical methods (**Figure S12**). A pair of well-defined redox peaks (Epa = 0.56 V, Epc = 0.22 V) was observed in the cyclic voltammetry curve of DOX/PGQD-HA modified glass carbon electrode (GCE) (**Figure S13a**). Based on the electrochemical response of DOX/PGQD-HA, a new model was fabricated to quantitatively calculate the DOX release ratio (**Figure S13b**).

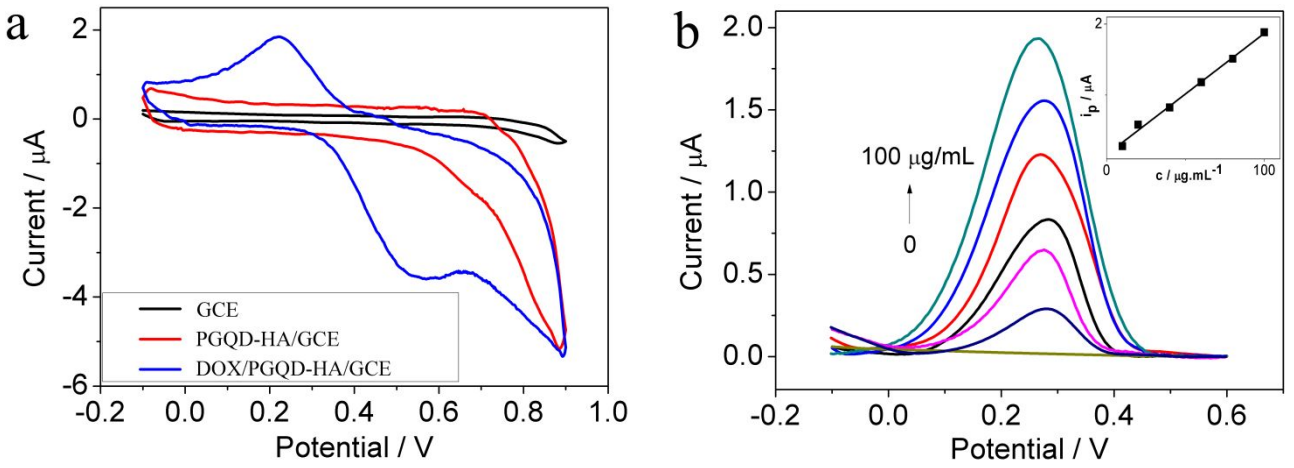

Figure S13. (a) Cyclic voltammetry curves of GCE (black), PGQD-HA/GCE (red) and DOX/PGQD-HA /GCE (blue) at a 100 mV/s scan rate in pH 7.4 phosphate buffer solution. (b) Square-wave voltammetry (SWV) response of DOX/PGQD-HA with different DOX concentrations. Inset is the calibration curve.

The results of our electrochemical method showed the release ratio of DOX in acidic surroundings was in agreement to that achieved by conventional UV-vis absorption spectroscopy (**Figure S14**). Under acidic conditions, the release rate was much higher than that at neutral conditions (**Figure S14**). This is attributed to the increased hydrophilicity of doxorubicin at a low pH via protonation of the NH_2 group of DOX, and thus subsequently weakens the hydrophobic interactions between the GQD surface and DOX.

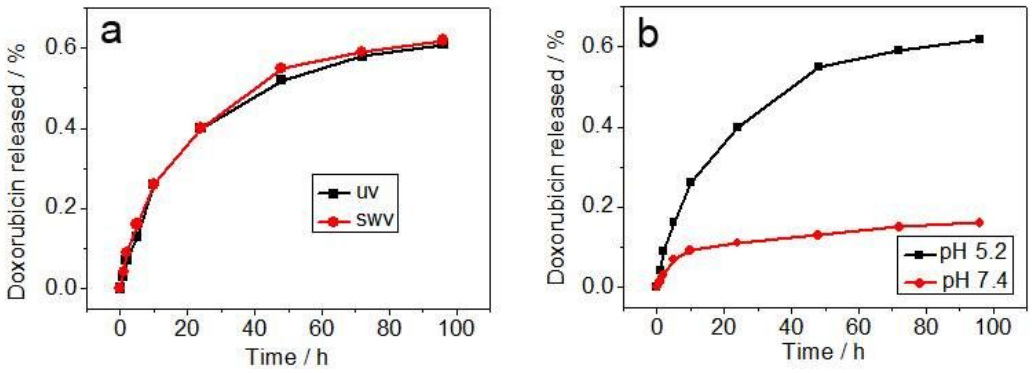

Figure S14. (a) DOX release from PGQD-HA achieved by UV spectrum (black) and electrochemistry measurement (red) in buffers at pH 5.2. (b) DOX release from PGQD-HA in buffers at pH 5.2 (red) and pH 7.4.

7. Isotherms characterizing adsorption of DOX onto GQD

The isotherms characterize adsorption of DOX onto the prepared GQD are shown in **Figure S15**. To compare extent of adsorption at different temperatures, adsorption isotherms at 299 K, 309 K and 319 K were obtained, respectively. An increase in the temperature from 299 to 319 K leads to

an increase in the adsorption capacity from 966.03 to 1243.1 mg/g at an initial concentration of 0.1 mg/mL. The saturated extent of adsorption increased as temperature ascended, indicating higher loading ratio of DOX on GQD at higher temperature. The extent of adsorption increased rapidly as equilibrium concentration rose, and reached its saturation at about 0.5 mg/mL DOX. The uptake increases with increasing temperature, this effect may be explained by the availability of more inactive sites caused by activation of the adsorbent surface at higher temperatures. The result indicates that the adsorption of DOX on GQD is endothermic in nature.

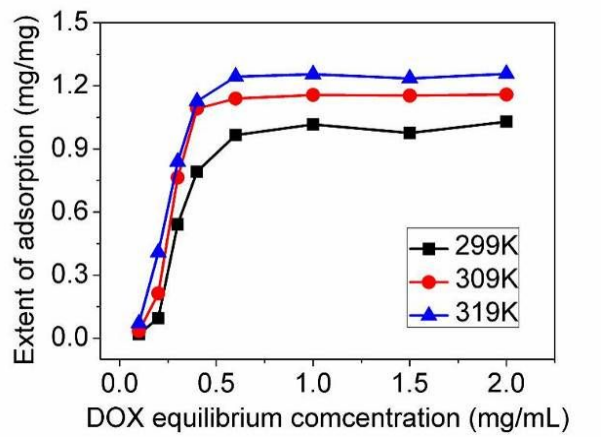

Figure S15. Adsorption isotherms of DOX on GQD at different temperatures.

8. Cell viability assay

To examine the viability of cells in the presence of the DOX/PGQD-HA, a 3-[4, 5-dimethylthialzol-2-yl]-2, 5-diphenyltetrazolium bromide (MTT, Sigma) assay was used. The assay was carried out in triplicate in the following manner: For the MTT assay, A549 cells were seeded in 96-well plates at a density of 1 × 104 per well in 100 μL of media, and were grown overnight. The cells were then incubated with various concentrations of GQD, PGQD-HA, and DOX/PGQD-HA at different times. The cells were then assayed for viability. To achieve this, Cell Titer 96® Aqueous One Solution reagent was added to each well. Cells were incubated for 4 h at 37 °C, in a humidified 5%CO2 atmosphere. The absorbance was measured at 490 nm, using a single-mode microplate reader (SpectraMax 190, Molecular Devices).

Mean absorbance for each drug and cell type was expressed as a percentage of the control untreated well absorbance. GQD and PGQD-HA nanoparticles do not significantly affect proliferation of A549 and MRC-5 cells with a concentration of 50 μg/mL **(Figure S16a)**, indicating the magnetofluorescent GQD can serve as an effective biological imaging platform with little cytotoxicity. For DOX loaded onto PGQD-HA, we incubated the complex with A549 cells at different concentrations for different days. Cellular viability gradually reduced as the enhancement of concentration and incubating time. MRC-5 cells were also incubated with DOX/PGQD-HA

conjugates with a maximum concentration. Compared with A549 cells, the cytotoxicity of DOX/PGQD-HA against MRC-5 cells is noticeably reduced. According to the CLSM and MRI results, this phenomenon is associated with the decreased uptake of DOX/PGQD-HA complex by MRC-5 cells. All these results demonstrate the designed delivery system has the potential to selectively kill cancer cells.

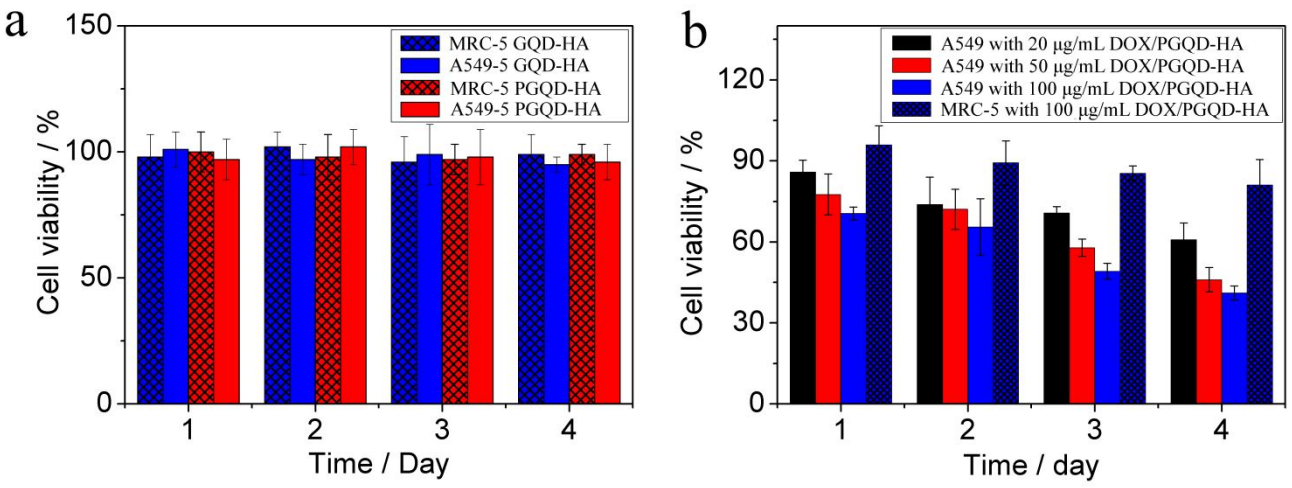

Figure S16. (a) Cell viability of GQD-HA (blue) and PGQD-HA (red) against A549 cells (unshaded) and MRC-5 cells (shaded). (b) Cell viability of DOX/PGQD-HA against A549 cells (unshaded) and MRC-5 cells (shaded) at different concentrations.